FULL PAPER

ADVANCED FUNCTIONAL MATERIALS

DOI: 10.1002/adfm.200700433

A Neutron and X-Ray Diffraction Study of Bioglass® with Reverse Monte Carlo Modelling**

By *Victoria FitzGerald*,* *David M. Pickup*, *David Greenspan*, *Gautam Sarkar*, *John J. Fitzgerald*, *Kate M. Wetherall*, *Rob M. Moss*, *Julian R. Jones*, and *Robert J. Newport*

A class of melt-quenched silicate glasses, containing calcium, phosphorus and alkali metals, and having the ability to promote bone regeneration and to fuse to living bone, creating strong implants with less danger of interfacial instability than previous materials, is produced commercially as Bioglass® and sold under the brand names of PerioGlas®, NovaBone® and NovaBone-C/M®. We have collected the first high energy X-ray and neutron diffraction data, on this important material in the hope of providing more direct experimental insight into the glass structure. Similarly, the first solid state MAS (magic angle spinning) ^{29}Si, ^{31}P, and ^{23}Na NMR data on the material is presented. The diffraction data has been modeled using the reverse Monte Carlo (RMC) method to allow the identification of the atomic-scale structural features present; the solid state NMR data is used explicitly within the model-building process as a constraint on the connectivity of the network. The ^{29}Si NMR suggests that the host silica network primarily consists of chains and rings of Q^2 SiO_4 tetrahedra, with some degree of cross linking as represented by the presence of Q^3 units. The diffraction-based RMC model suggests a Na–O distance of 2.35 Å and a corresponding coordination of ~6; the coordination number is supported by the ^{23}Na NMR data presented here which reveals that the likely sodium environment is six-coordinate in pseudo-octahedral arrangement. The RMC model provides evidence for the non-uniform distribution of Ca, which is in line with previous molecular dynamics simulation results, and the data is also suggestive of CaO as the associated structural motif within the high calcium content regions of the glass.

1. Introduction

Average life expectancy in the Western world has increased dramatically with better nutrition and improvements in medical care. To allow people to remain active, and to contribute to society for longer, the need for new materials to replace and repair worn out and damaged tissues becomes ever more important. The Kent team has joined a program of study underway in the USA involving the company who produce a number of products made from Bioglass®. Bioglass® is a bioactive material that has been shown to form a bond with bone when implanted into a bony defect.[1,2] There have been numerous studies during the past 20 years that have attempted to correlate the chemistry of these Bioglass materials with their reactivity and the corresponding reactions with tissue in the body.[3–5] Generically, these novel glasses have become known as bioactive glasses. While a great deal has been learned about the surface reactivity with respect to compositional differences and the resulting response in the body, the atomic-scale structural details of these materials have not been extensively studied.

The family of bioactive glasses are, in essence, calcium silicate glasses with additional alkali and alkaline earth modifiers. The study of atomic-scale structure undertaken hitherto is largely limited to electron microscopy and IR spectroscopy, together with exploratory molecular dynamics, MD, simulation. We have collected the first high energy X-ray and neutron diffraction data, and solid state MAS (magic angle spinning) ^{29}Si, ^{31}P, and ^{23}Na NMR data on this important material in the hope of providing more direct experimental insight into the glass structure. The experimental data has been modeled using the reverse Monte Carlo (RMC) method, primarily as an aid to the interpretation of atomic-scale structural features present in the diffraction-derived pair correlation functions. For a relatively complex system such as this multicomponent glass, no one structural probe is able to provide a definitive structural model. Complementary methods need to be employed within a materials-centred methodology. Here we have employed both X-ray and neutron diffraction, alongside solid state NMR measurements using several key nuclei.

[*] V. FitzGerald, Dr. D. M. Pickup, K. M. Wetherall, R. M. Moss, Prof. R. J. Newport
School of Physical Sciences, University of Kent at Canterbury
Canterbury, CT2 7NR (UK)
E-mail: vf22@kent.ac.uk
Dr. D. Greenspan
Novamin Technology Inc.
13859 Progress Blvd., Alachua, FL 32615 (USA)
Dr. G. Sarkar, Dr. J. J. Fitzgerald
Department of Chemistry and Biochemistry, South Dakota State University
Brookings, SD 57007 (USA)
Dr. J. R. Jones
Department of Materials, Imperial College London
London, SW7 2AZ (UK)

[**] Drs. M. A. Roberts and A. Lennie are thanked for their help in using the 9.1 diffractometer at the SRS (CCLRC, UK). Prof. Alex Hannon is thanked for his help in using GEM at ISIS (CCLRC, UK). VF thanks the EPSRC and the University of Kent for her studentship.

ADVANCED FUNCTIONAL MATERIALS

There is a significant difference between the experimentally determined X-ray and neutron structure factors due to the differences in weighting factors derived using Equation 4, and which are shown graphically for each partial in Figure 1.

This figure demonstrates that X-ray diffraction data are to be preferred for studying the intermediate-range order of oxide glasses, because the weighting factors of the Si···Si, Si···Ca and Ca···Ca correlations, which are strongly related to intermediate-range order of these glasses, are relatively larger for X-rays than for neutrons. The figure also shows that the neutron data is better conditioned for obtaining data associated with O···O correlations (as well as for the provision of better resolved real-space data *per se* as per Eq. 6). To this information we add the element-specific short-range data derived from NMR; the ability to use all of this data simultaneously within a single cogent model building process leads to the generation of a robust structural picture of the material.

A detailed quantitative knowledge of the structure of these bioactive glasses is a pre-requisite for a full understanding of how changes in materials processing, composition etc. affects *in vitro* reactivity and the resultant *in vivo* response of the body. For example, the rate of dissolution of the glass, and in particular the rate at which Ca, P, Si ions enter the fluid surrounding the glass, is known to be a crucial factor in the gene switching needed to initiate the required oesteoblast activity.[6,7] Thus, one may immediately ask what it is about the environment of the Ca site within the glass that allows it to be facile in this way. Similarly, Na would in silica act as a network modifier (increasing the solubility of the glass as a result of reduced network connectivity), but its role may be significantly altered in the presence of phosphate moieties. It is on this basis that elucidation of the atomic-scale structure of the glass will help to make it possible to improve the functional performance of bioactive glasses via controlled discrete tailoring.

2. Results and Discussion

The ^{29}Si, ^{31}P, ^{23}Na NMR spectra are shown in Figure 2.

The ^{29}Si spectrum exhibits one broad and asymmetric peak which can be deconvolved by Gaussian fitting into two resonance peaks centered at –88.1 and –80.4 ppm. ^{29}Si NMR spectra from oxide materials are normally discussed in terms of Q^n units, which describe the connectivity of the SiO_4 tetrahedra that make up the structure. Thus, Q^0, Q^1, Q^2, Q^3, and Q^4 units

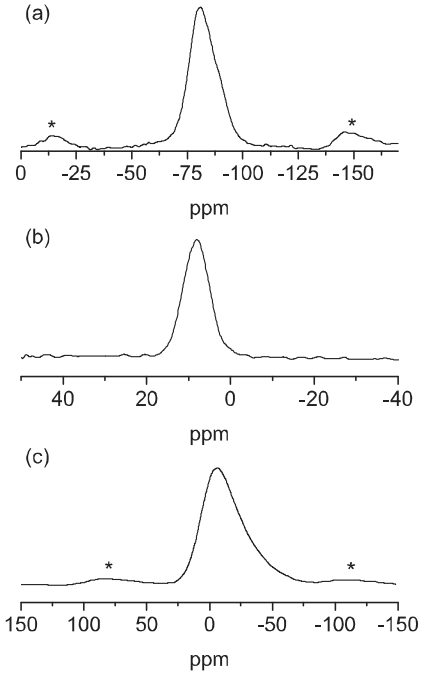

Figure 2. Solid state MAS NMR spectra: a) ^{29}Si, b) ^{31}P, and c) ^{23}Na.

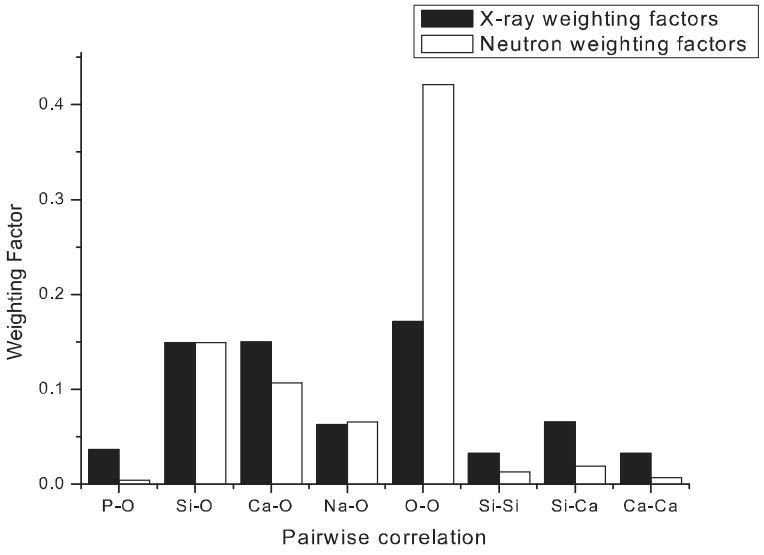

Figure 1. Histogram comparing relative X-ray and neutron scattering weighting factors for each pair correlation peak analyzed in the fitting process (the total areas have in both cases been normalized to unity).

represent SiO_4 groups connected to 0, 1, 2, 3, or 4 other such groups, respectively. The two peaks observed in the ^{29}Si NMR spectrum from Bioglass® at –88.1 and –80.4 ppm are assigned to Q^3 and Q^2 units, respectively.[8,9] The relative intensity (from Gaussian fitting) of the Q^3 and Q^2 peaks is 31 % and 69 %, respectively. This result therefore suggests that the silica network of the structure mostly consists of chains and rings of Q^2 SiO_4 tetrahedra with some degree of cross linking as represented by the presence of the Q^3 units.

The ^{31}P NMR spectrum consists of one broad resonance at 8.1 ppm. This can be assigned to the presence of phosphorus in an orthophosphate environment[8,9] and thus suggests that phosphorus exists in isolated PO_4^{3-} anions in the structure, thereby removing sodium and calcium cations from a network-modifying role in the silicate network.[8] In fact, the chemical shift of the phosphorus resonance is midway between that of $Ca_3(PO_4)_2$ (0 ppm) and that of $Na_2(PO_4)$ (15.6 ppm),[10] providing evidence that the

PO_4^{3-} anions are associated with the metal cations. In a molecular dynamics, MD, study[11] performed on Bioglass® the presence of some Q^1 species were suggested (~33 %), and also some Q^2 (~2 %), the Q^2 relating specifically to the presence of P–O–Si bonds. FTIR studies of the sol-gel synthesized variants of Bioglass® were also interpreted as showing evidence of labile P–O–Si bridge.[12] However, these unstable P-containing bridges are present only on the surface of the sol-gel materials after dehydration; indeed, exposure of the sol-gel material to atmospheric moisture was sufficient to open the bridges. Thus, if such bridges are present in a high-density (i.e., pore-free) melt-quenched (i.e., arguably more thermodynamically stable) glass such as that studied here, their concentration would probably be low by comparison. This conjecture would seem to be in agreement with optical spectroscopic data on Bioglass®, collected by the same group who studied the sol-gel material, which showed no evidence of P–O–Si bonds.[13] The new NMR data presented herein cannot rule out the presence of low levels of P–O–Si bridges, but given that the spectra may be fitted satisfactorily without the need to include Q^1 or Q^2 species we are forced to conclude that their levels must be significantly less than those suggested by MD. The experimental data is of course limited by its intrinsic sensitivity, and a small fraction of Q^1 species may therefore be present – but, taken together, the NMR and optical data would seem to rule out the ~33 % postulated as a result of the MD study. Given the labile nature of Si–O–P bridges, this is an important observation in the context of the dissolution of Bioglass® in physiological fluids.

The ^{23}Na NMR spectrum exhibits one broad asymmetric resonance at –6.1 ppm. The asymmetry is due to residual second-order quadrupolar interactions which are not completely removed under MAS conditions.[8] Sodium ions present in different coordination environments have been correlated with distinct but overlapping solid-state ^{23}Na NMR chemical shifts or chemical shift ranges (4-coordinate sodium ca. –50 ppm, 5-coordinate sodium ca. –21 ppm and 6-coordinate sodium from ca. –7.2 ppm to –3.0 ppm) for a number of compounds.[14,15] The ^{23}Na NMR chemical shift for Bioglass®reveals that the likely sodium environment is six-coordinate in a pseudo-octahedral NaO_6 arrangement, although the presence of five-coordinate Na^+ ions cannot be completely excluded.

This direct experimental information is now utilized to produce an RMC model. In particular, the ^{29}Si NMR data was used to determine the Q speciation of the Si network. In each of the models generated, a constraint was included on the Si to ensure that the model contained 31 % Q^3 units and 69 % Q^2 units. Also, a constraint was added to the P in terms of its bonding to oxygen to ensure that it was present in an orthophosphate environment. These constraints were subsequently varied to examine the effect they had on the overall model. Changes to the constraints, within a reasonable limit, had little effect on the structural statistics derived from the final resultant model (i.e., after it had also been constrained by the diffraction data, see below), indicating that the model structure is itself robust against errors in the data. It also reinforces the important fact that 3-D RMC models, derived as they are from one-dimensional data, cannot be regarded as unique solutions. Due to the slightly different compositions of the two samples shown in Table 1, two separate models were generated initially – one for each of the powdered sample for the X-ray diffraction data and the glass rod for the neutron diffraction data.

Table 1. Sample characterization: density measurements are based on helium pycnometry; X-ray fluorescence was used to provide compositional analysis. The compositions used in the RMC model were obtained on the basis of XRF measurements, charge balancing and solid state NMR data.

	Bioglass® powder sample for XRD	Bioglass® rod sample for ND
Density [g cm^{-3}]	2.709	2.700
Density atoms [Å^{-3}]	0.077	0.077
Composition XRF [mol-%]		
CaO	26.9	26.2
SiO_2	46.1	47.2
P_2O_5	2.60	3.15
Na_2O	24.4	23.8
Composition of Model [mol-%]		
CaO	25.9	26.2
SiO_2	48.0	47.2
P_2O_5	2.60	3.15
Na_2O	23.1	23.8
Side Length of RMC box [Å]	32.78	32.77

The diffraction data and the corresponding RMC fits for each data set are shown in Figure 3 ($S(Q)$'s) and Figure 4 ($T(r)$'s).

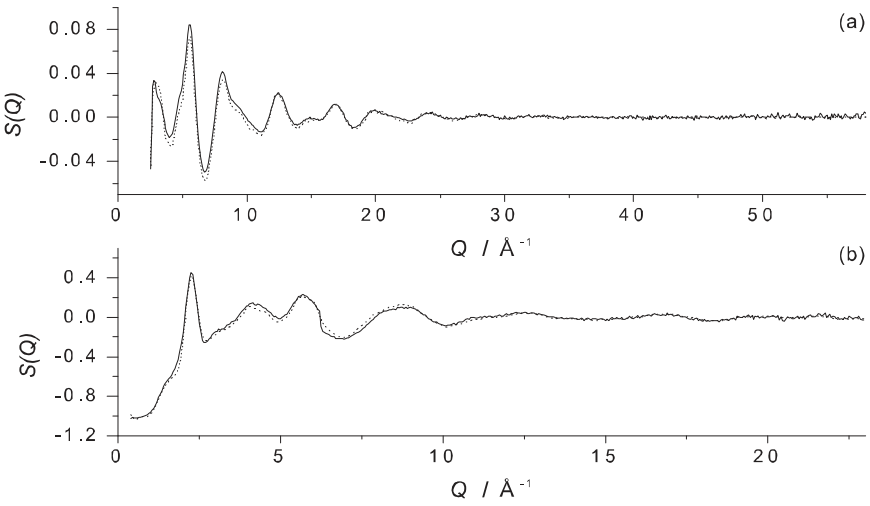

Figure 3. a) Neutron diffraction data from the Bioglass® sample: Q-space structure factor $S(Q)$ (solid line) together with RMC fit (dotted line); and b) high energy X-ray diffraction data from the Bioglass® sample: Q-space structure factor $S(Q)$ (solid line) together with RMC fit (dotted line).

ADVANCED FUNCTIONAL MATERIALS

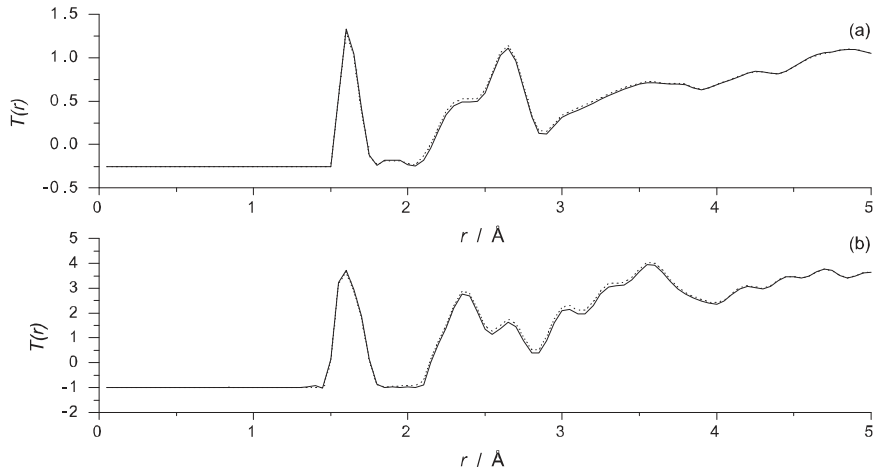

Figure 4. a) Neutron diffraction data from the Bioglass® sample: pair distribution function $T(r)$ (solid line) together with RMC fit (dotted line); and b) high energy X-ray diffraction data from the Bioglass® sample – pair distribution function $T(r)$ (solid line) together with RMC fit (dotted line).

After careful examination of the closely similar partial pair correlations and model structures resulting from each RMC model, it was considered appropriate to average the partial pair correlation functions, and thereafter to treat the data as coming from one combined model. In Figure 5, nine principal partial $T_{ij}(r)$ functions output from the RMC models are shown.

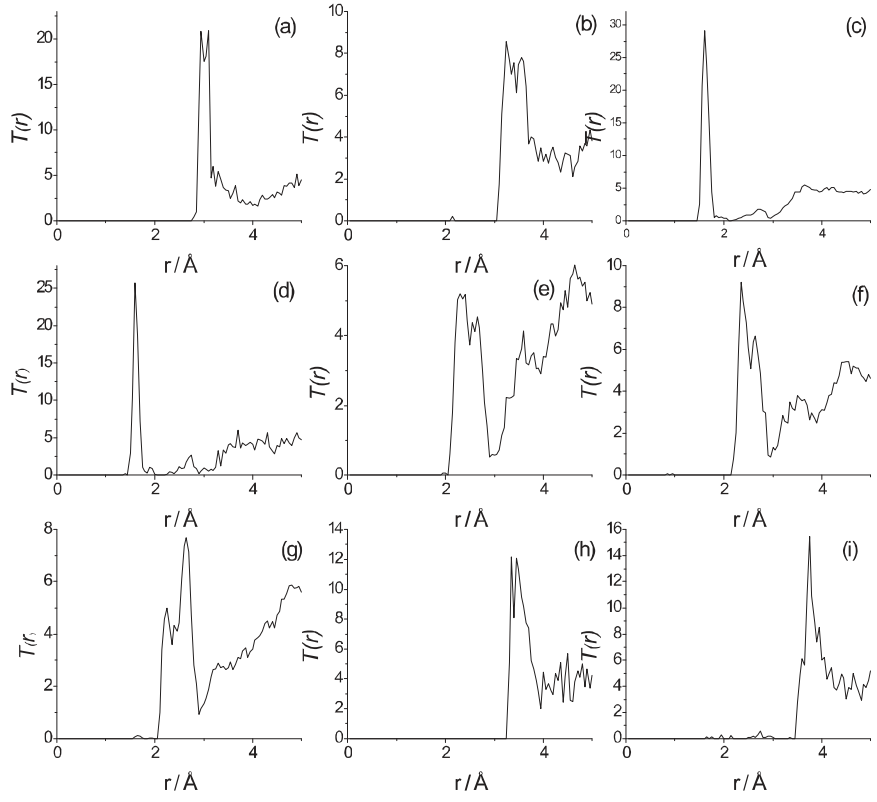

Figure 5. RMC partial $T_{ij}(r)$ functions, a) Si···Si, b) Si···Ca, c) Si–O, d) P–O, e) Ca–O, f) Na–O, (g) O···O, (h) Ca···Ca, (i) Na···Na.

The parameters obtained from the RMC model are shown in Table 2.

RMC modeling provides a non-unique 3-D model of a structure which is consistent with all the constraints applied; it is an extremely useful heuristic tool but, as with all empirical methods, care must be taken in order to avoid over-interpretation of the results. Due to the very small amount of phosphorous present (1.8 at %, corresponding to only ~50 P atoms within the model), very little genuinely reliable information about the phosphorous environment within the glass network beyond the first oxygen shell. Thus, one cannot place any weight on the details of the P···X bridging correlations within the RMC model, and these parameters have been included at the bottom of Table 2 for completeness only. Therefore, whilst the model is seen to contain some Si–O–P bridges, their numbers are not statistically significant.

Given that the ^{31}P NMR results are consistent with orthophosphate (Q^0) units, and that the data indicates that the PO_4^{3-} anions are associated with the metal cations, one would expect to observe a P–O_{nb} bond at ~1.53 Å as found in $Ca_3(PO_4)_2$ [16] and in $Na_2(PO_4)$.[17] Both of these materials exhibit one P–O_{nb} bond as long as ~1.58 Å however this does not agree with the four P–O_{nb} bonds at ~1.6 Å shown in Table 2. Despite the statistical limitations of our model, we nevertheless note the fact that the RMC model gave a P–O_{nb} coordination of ~3.9 and a P–O_b coordination of ~0.03. This would indicate the predominant presence of orthophosphate (Q^0) units within the model, as shown by the NMR data (and independent optical spectroscopy data,[13]) and explicitly incorporated into our model-building process. The associated modeled bond distance of ~1.6 Å is more usually associated with P–O_b bonds,[18] but more probably indicates that the dominant Si–O correlation at 1.6 Å is affecting our ability accurately to fit the relatively very weak P–O contribution.

The partial pair correlation functions derived from the RMC model place the Si–O peak at 1.61 Å with a coordination of slightly less than 4, as expected in silica based materials.[19] The Ca–O partial is seen to be an asymmetric feature in Figure 6 centered at ~2.5 Å but extending from 2.05 Å to 2.90 Å with two partially resolved peaks, and a total coordination number of ~5. This is in good agreement with previous data obtained in a recent

Table 2. Structural parameters obtained from RMC modelling; because there are relatively few P atoms in the RMC box, the parameters returned are regarded as having qualitatively less meaning. (s is the full width half maximum of the peaks).

Sample	Correlation	*R* [Å]	*N*	*σ* [Å]
45S5 RMC	Si-O	1.61	~3.7	0.06
partials	Ca-O	2.31, 2.59	~4.9	0.24
	Na-O	2.35	~6.0	0.16
	O···O	2.64	~3.0	0.15
	Si···Na	2.96	~4.0	0.31
	Si···Si	3.03	~2.3	0.10
	Ca···Na	3.05	~3.6	0.16
	Si···Ca	3.25	~1.6	0.26
	Ca···Ca	3.48	~1.7	0.20
	Na···Na	3.75	~3.3	0.26
	P-O	1.60	~3.9	0.04
	P···P	*2.9*	*~0.2*	*0.1*
	P···Ca	*3*	*~2.6*	*0.6*
	P···Na	*3*	*~4.5*	*0.4*
	P···Si	*3*	*~0.3*	*0.1*
	Si···P	*3*	*~2.6*	*0.1*

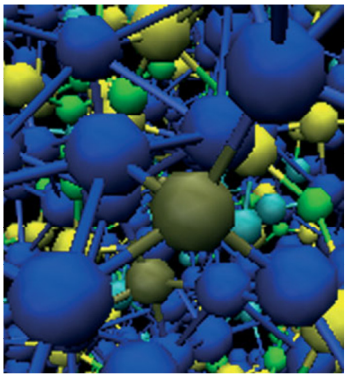

Figure 6. Example of phosphorous in an orthophosphate environment. P atom (brown) connected to four O_{nb} atoms (blue)

neutron diffraction with isotopic substitution experiment undertaken on an analogous bioactive calcia-silica sol-gel glass,[20] and also with a corresponding molecular dynamics study.[21] These results are in good agreement with bond distances obtained from molecular dynamics studies of the same material.[11] The molecular dynamics results showed the Si–O peak at 1.59 Å, the Ca–O peak at 2.29 Å and the Na-O peak at 2.34 Å. The model Na–O partial pair correlation function in this study indicates a distance of 2.35 Å, which is consistent with previous measurements,[22] and a coordination of ~6, agrees with the ^{23}Na NMR data which indicated that the sodium environment is six-coordinate within a pseudo-octahedral NaO_6 arrangement.

The model O···O partial pair correlation is found as expected in a silica based material, and as found in the molecular dynamics study,[11] at 2.64 Å, with a coordination of ~3. The O–Si–O coordination number would tend towards six in a fully densified silica network, but is reduced here due to the presence of O_{nb} atoms. This would imply that the presence of Ca and Na is causing significant disruption to the base silica network.

The Si···Si, Si···Ca, and Ca···Ca partial pair correlation functions derived from the RMC model give peak distances of 3.03, 3.25, and 3.48 Å respectively. The Si···Si coordination number of just above 2 agrees with the fact that Si is mostly present in Q^2 units.

Figure 7 shows an example of silica tetrahedra and Figure 6 shows a phosphorous tetrahedra from one of the RMC models after fitting to the data.

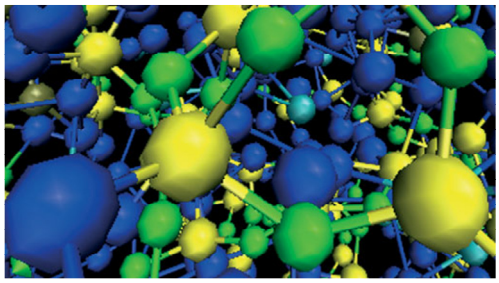

Figure 7. Example of Si atom (yellow) connected to three O_b atoms (green) and one O_{nb} atom (blue).

The model shows some evidence of a heterogenous distribution of calcium ion, i.e., clustering. This spatial clustering has been observed previously in a MD study.[11] The nearest neighbors distance of 3.48 Å obtained from the empirical RMC model, is significantly less than the Ca···Ca distance of 5.2 Å obtained by assuming a completely homogeneous (i.e., gas-like) Ca distribution. Also, the coordination expected for a homogenous distribution of ions, given by $N_{Ca\cdots Ca}(hom.) = (4/3)\pi R_c^3 \rho(\mathrm{Ca}) - 1$, where R_c is the first minimum in the partial $T(r)$ function, $T_{Ca\cdots Ca}(r)$, and ρ(Ca) is the number density of Ca in our model, predicts a Ca···Ca coordination of ~0.9, whereas the RMC model returns ~1.7. There is some uncertainty associated with these estimates, associated with the need to define the first minimum in the $T(r)$, but not enough to obviate the overall conclusion. Thus, both approaches offer clear evidence for calcium clustering in Bioglass®. A comparable effect has previously been observed in analogous samples of sol-gel bioactive glasses, wherein it was suggested that clustering occurred, on the surfaces of the glass, as the concentration of Ca in the samples increased (and as a consequence influenced the acid/base properties of the bioactive glass surface).[23] The results presented herein are necessarily limited to the suggestion that Ca clusters exist, *per se*; given that Bioglass® is a high-density melt-quenched glass, the question of surface segregation does not arise. Clustering does however have an immediate consequence for the observed bioactivity of the material in the sense that diffusion/dissolution pathways will be heavily influenced by the existence of connected volume elements of high Ca concentration within a modified silicate network.

Similarly, the nearest neighbor Na···Na correlation shell is determined to be centered at 3.75 Å, compared to a calculated

ADVANCED FUNCTIONAL MATERIALS

distance of 4.3 Å if one assumes a completely homogeneous Na distribution. Likewise, the coordination number of ~3.3 derived from the RMC model may be compared with the value of ~2.9 expected for a homogeneous distribution. Thus, there is again some evidence, albeit weaker than in the case of Ca, for the possibility of sodium clustering. In the MD study of Bioglass® referred to above,[11] it was suggested that Ca dominates the coordination of the orthophosphate groups.

3. Conclusions

Given that the bioactivity of the glass is intimately related to – indeed, determined by – the release of ions from the glass as the dissolution process takes place in physiological fluids, and the consequential interplay between surface charge on the glass and fluid pH, it is of central importance that one understands the local environment of the various chemical species. Interatomic bonds must be broken (and sometimes re-arranged) for this process to occur: an understanding of the atomic-scale structure of the glass is therefore vital. Of particular importance is the role of Na as a network terminator (since it is likely to affect overall dissolution rates) and Ca as the network modifier having the most profound biological affect in terms of its gene-switching role. Additionally, labile species such as the Si–O–P bridges postulated by MD studies would, if present, be an important factor in the determination of surface chemistry – i.e., of dissolution reactions in physiological fluids.

A model has been generated and interpreted on the basis of the first high energy X-ray and neutron diffraction study and the first multi-nucleus solid state NMR data on Bioglass®. The diffraction data, analyzed using an RMC model which explicitly incorporates the results of the solid state NMR data, show a significantly disrupted silica network.

The ^{29}Si NMR suggests that the host silica network primarily consists of chains and rings of Q^2 SiO_4 tetrahedra, with some degree of cross linking as represented by the presence of Q^3 units. The ^{31}P NMR indicates that phosphorus exists as isolated PO_4^{3-} anions in the structure, which will remove sodium and calcium cations from a network-modifying role in the silicate network. However, there is a possibility that a small number of pyrophosphate units are present. No confirmation of the postulated presence of significant concentrations of Si–O–P bridges was discerned.

The diffraction data show a broad Ca-O pair correlation at ~2.05–2.90 Å, with a total coordination of ~5, which is consistent with previous NDIS and MD results from an analogous bioactive calcia-silica sol-gel glass. The diffraction data suggest a Na-O distance of 2.38 Å and a corresponding coordination of ~6, which is in good agreement with previously published values; the coordination number is supported by the ^{23}Na NMR data presented here, which reveals that the likely sodium environment is six-coordinate in pseudo-octahedral NaO_6 arrangement, although there is the possibility of the presence of five-coordinate Na^+ ions.

There is evidence of a non-homogeneous distribution of Na within the glass, which is important in the context of the relatively slow dissolution of the modified silica network. The data provides evidence of Ca clustering, which is consistent with the predictions of a molecular dynamics simulation for a similar sample, and also implies the presence of CaO as the structural motif. This latter observation is of direct relevance to the understanding of the facile nature of Ca within such glasses which gives rise to its relatively rapid diffusion from the solid into solution (and therefore to its behavior in terms of the material's overall bioactivity).

4. Experimental

Sample Preparation: The samples of Bioglass® for X-ray diffraction and solid state NMR experiments were supplied by Novamin Technology, Inc. (Alachua, Florida). The samples were in granular form; their composition and density are reported in Table 1. The Bioglass® sample for neutron diffraction was supplied by Imperial College London, prepared in the same fashion, but caste in the form of a solid glass rod, the composition and density are reported in Table 1. Composition analysis for both sets of samples was performed using a Bruker S4 X-ray fluorescence instrument. Density measurements were based on helium pycnometry performed using a Quantachrome multipycnometer.

X-ray and Neutron Diffraction Methods and Data Analysis: The high energy X-ray diffraction (HEXRD) data was collected on Station 9.1 at the synchrotron radiation source (SRS), Daresbury Laboratory, UK. The finely powdered samples were enclosed inside a 0.5 mm thick circular metal annulus by kapton windows and mounted within a flat-plate instrumental set-up. The wavelength was set at λ = 0.4875 Å, and calibrated using the K-edge of a Ag foil; this value was low enough to provide data to a high value of wavevector transfer ($Q_{max} = 4\pi\sin\theta_{max}/\lambda \sim 23$ Å^{-1}). The data were corrected using a suite of programs written in-house, but based upon the methodology of Warren [24].

The initial stage of analysis of X-ray diffraction data from an amorphous material involves the removal of background scattering, normalization, correction for absorption and inelastic scattering, and subtraction of the self-scattering term [25]. No correction was made to account for multiple scattering since it is a negligible effect in HEXRD from thin samples having low sample attenuation.

The neutron diffraction (ND) data was collected on the GEM total scattering instrument at the ISIS pulsed muon and neutron source at the Rutherford Appleton Laboratory. The data was reduced using the program *gudrun* [26], to produce a corrected differential cross-section curve. The data are corrected for absorption and multiple scattering, and then are normalized to vanadium – an almost wholly incoherent scatterer – and combined to produce a final structure factor, $S(Q)$, on an absolute cross-section scale.

Both the XRD and ND methods are governed by the same generic physical principles. After data reduction and the consequent generation of the structure factor, $S(Q)$, one may derive the associated real space pair correlation function, $T(r)$, by Fourier transformation via the following equation:

$$T(r) = \frac{2}{\pi}\int_0^\infty QS(Q)\sin(Qr)dr + T^0(r) \quad (3)$$

For multicomponent systems, such as under discussion here, $T(r)$ may also be defined in terms of the partial correlation functions, $T_{ij}(r)$, for pairs of atomic species i and j as

$$T(r) = \sum_{i,j} n_i n_j Z_i Z_j T_{ij}(r) \quad (4)$$

and $T^0(r)$ is defined as

$$T^0(r) = 4\pi r\rho(\textstyle\sum_i n_i Z_i)^2 \quad (5)$$

where ρ is the atomic number density; n_i is the fraction of atom type i, and Z_i is the corresponding atomic number (X-rays) or coherent scattering length (b_i) (neutrons), for. It is possible to obtain structural information from $T(r)$ (e.g., bond lengths, coordination numbers etc.) via a modelling process.

We note that the effective resolution of features within $T(r)$ is

$$\Delta r \sim \frac{2\pi}{Q_{max}} \quad (6)$$

^{29}Si, ^{31}P, and ^{23}Na MAS NMR: The ^{23}Na, ^{29}Si, ^{31}P NMR spectra were measured on a Bruker ASX-400 spectrometer (9.45 T) using a Bruker HP WB 73 A MAS probe at 105.857, 79.49, and 16 997 MHz, respectively. The ^{23}Na and ^{31}P NMR measurements were made using a 4 mm probe (typically 0.14 g sample size) at 13.0 to 13.5 kHz sample spinning, while the ^{29}Si NMR measurements were made using a 7 mm probe (0.64 g sample) at 7 kHz sample spinning speed. The ^{29}Si and ^{31}P NMR spectra were acquired using a single-pulse sequence. The ^{23}Na NMR spectrum was acquired using a spin-echo pulse sequence to suppress the effect of "probe ringing" and to obtain a flat baseline. An echo time of one rotor period (1τ = 76.92 μs) was used. The chemical shifts (δ) were referenced to 1 M NaCl for ^{23}Na and 85 % H_3PO_4 for ^{31}P (0 ppm). The ^{29}Si spectrum was referenced to a secondary standard of kaolinite (δ = –91.5 ppm relative to tetramethylsilane as its primary standard). The 90° pulse widths for ^{29}Si and ^{31}P NMR were 5 μs and 3.5 μs, respectively. A selective pulse width of 2.5 μs (half of the liquid 90° pulse length) was used for ^{23}Na to observe the central transition (½ ↔ –½). The recycle delay times used for ^{23}Na, ^{31}P and ^{29}Si were 1 s, 3 s, and 60 s, respectively. These values are sufficiently long to allow the complete relaxation necessary to obtain quantitative information about spin populations. The total number of scans used for ^{23}Na, ^{29}Si, and ^{31}P NMR spectra were 512, 256, and 5000, respectively.

RMC Method: RMC is a method for producing three-dimensional models of a structure that agree quantitatively with available data. A starting model of a material, composed of atoms in a box at the correct density and composition, is modified by random processes in such a way as to improve the agreement between a set of experimental data and the equivalent function calculated from the model. The structure is modified in this way until it agrees with the experimental data within some satisfactory measure of the error. A full description of the RMC method can be found in a paper by McGreevy et al. [27]. Using the diffraction data, together with a set of constraints derived from our NMR data and from prior chemical knowledge, a three-dimensional model has been produced for the sample studied herein. The RMC model box for the Bioglass® is made up of ~3000 atoms, with correct atomic number density and composition obtained from pycnometry measurements and X-ray fluorescence composition analysis respectively, as per Table 1. Charge-balancing was also used as an aid to building a box with the correct composition (especially important in terms of refining the oxygen content). The size chosen for the associated cubic box, determined in order to match the measured density, is also shown in Table 1.

In order to obtain as a starting configuration the four oxygen atoms around each silicon atom suggested on the basis of prior chemical knowledge, a random array of Si atoms was produced first which were moved out to a minimum distance of 2.85 Å, and then O atoms were inserted at the medium distance between each pair of neighboring Si atoms. The P atoms, and corresponding additional O atoms, were then added to this pseudo-silica array at random positions. The details of the bonding constraints imposed via the RMC algorithm were decided upon using the solid state NMR values for Q speciation (i.e., the relative numbers of O_b and O_{nb}). Specifically, for the Q^2 units, the atoms in the box were moved such that each silicon atom was coordinated to two O_b and two O_{nb} (and each O was coordinated to only two other atoms, neither of which could be another O). After the base silica network was produced and phosphorous was included, the Ca and Na atoms were added randomly. Within this initial phase of defining the configuration of the box, there are two other considerations of importance: the definition of distances of closest approach for each pair of atom types, and the choice and use of the target goodness-of-fit value, σ. The latter parameter, along with the magnitude of the individual atom movements at each step, may be varied to help optimize the speed with which the constraints (and eventually the experimental data) are satisfied; ultimately however its value is chosen in order to correspond as far as is practicable with the average uncertainty associated with the experimental data. Distances of closest approach are empirically defined using the $T(r)$ derived from the HEXRD and ND data by direct Fourier transformation as far as is possible. For those pairwise correlations that are not adequately resolved it is found that an iterative approach is required, employing whatever starting values might be available in the literature (e.g., for crystalline analogues or comparable amorphous systems). Naturally, this tends to be more problematic in the case of the HEXRD data since the real-space resolution is not as favorable as it is in the context of the ND data. As a guiding principle, the largest value of the distance for closest approach consistent with obtaining approximately Gaussian correlation peaks was used; e.g., care was taken to avoid setting values that resulted in having atoms 'pile up' against limiting distances as the algorithm attempts to fit the model to the experimental data. The values adopted in the present study are shown in Table 3.

Table 3. Distances of closest approach used during the RMC modelling process.

	Distance [Å]
Si···Si	2.80
Si- O_b	1.45
Si-O_{nb}	1.45
Si···P	2.90
Si···Ca	3.10
Si···Na	2.90
O_b···O_b	2.10
O_b···O_{nb}	2.10
O_b···P	1.35
Ca-O_b	2.10
Na-O_b	2.20
O_{nb}···O_{nb}	2.10
P-O_{nb}	1.35
Ca-O_{nb}	2.10
Na-O_{nb}	2.20
P···P	2.70
P···Ca	2.90
P···Na	2.90
Ca···Ca	3.30
Ca···Na	3.00
Na···Na	3.50

Only when the initially random box of atoms satisfied the above constraints to a satisfactory level (> 98 %) was the data added as the final additional constraint. After the ratio of successful to failed moves of the atoms within the box falls to its equilibrium value, about which it will fluctuate, the model was deemed to have reached a dynamic equilibrium. At this point, assuming an overall examination of the structure is satisfactory (e.g., that the SiO_4^{2-} units assume a roughly tetrahedral shape) it becomes possible to interrogate the model in order to generate information on possible partial pairwise correlations, $T_{ij}(r)$ – i.e., those correlations consistent with the experimental data.

Received: April 16, 2007
Revised: August 28, 2007
Published online: November 28, 2007

ADVANCED FUNCTIONAL MATERIALS

[1] L. L. Hench, R. J. Splinter, W. C. Allen, T. K. Greenlee, *J. Biomed. Mater. Res. Symp.* **1971**, *5*, 117.
[2] A. E. Clark, L. L. Hench, *J. Biomed. Mater. Res.* **1976**, *10*, 161.
[3] L. L. Hench, Ö. Andersson, in *An Introduction to Bioceramics*, Vol. 1 (Eds: L. L. Hench, J. Wilson), World Scientific, Singapore **1993**, p. 45.
[4] O. H. Andersson, I. Kangasniemi, *J. Biomed. Mater. Res.* **1991**, *25*, 1019.
[5] W. Cao, L. L. Hench, *Ceram. Int.* **1996**, *22*, 493.
[6] I. D. Xynos, A. J. Edgar, L. D. Buttery, L. L. Hench, J. M. Polak, *J. Biomed. Mater. Res.* **2001**, *55*, 151.
[7] I. D. Xynos, A. J. Edgar, L. D. Buttery, L. L. Hench, J. M. Polak, *Biochem. Biophys. Res. Commun.* **2000**, *276*, 461.
[8] M. W. G. Lockyer, D. Holland, R. Dupree, *J. Non-Cryst. Solids* **2005**, *351*, 173.
[9] I. Elgayar, A. E. Aliev, A. R. Boccaccini, R. G. Hill, *J. Non-Cryst. Solids* **1995**, *188*, 207.
[10] I. L. Mudrakovskii, V. P. Schmachkova, N. S. Kotsarenko, V. M. Mastikhin, *J. Phys. Chem. Solids* **1986**, *47(4)*, 335.
[11] A. Tilocca, A. N. Cormack, N. H. de Leeuw, *Chem. Mater.* **2007**, *19*, 95.
[12] M. Cerrutti, G. Magnacca, V. Bolis, C. Marterra, *J. Mater. Chem.* **2003**, *13*, 12709.
[13] M. Cerrutti, C. L. Bianchi, F. Bonino, A. Damin, A. Perardi, C. Marterra, *J. Phys. Chem. B* **2005**, *109*, 14496.
[14] H. Koller, G. Engelhardt, A. P. M. Kentgens, J. Sauer, *J. Phys. Chem.* **1994**, *98*, 1544.
[15] J. F Stebbins, X. Y. Xue, *Phys. Chem. Miner.* **1993**, *20*, 297.
[16] M. Yashima, A. Sakai, T. Kamiyama, A. Hoshikawa, *J. Solid State Chem.* **2003**, *175*, 272.
[17] R. J. Harrison, A. Putnis, W. Kockelmann, *Phys. Chem. Chem. Phys.* **2002**, *4*, 3252.
[18] U. Hoppe, G. Walter, A. Barz, D. Stachel, A. C. Hannon, *J. Phys. Condens. Matter* **1998**, *10*, 261.
[19] A.C. Wright, in *Experimental Techniques of Glass Science* (Eds: C. J. Simmons, O. H. El-Bayoum), American Ceramic Society, Westerville, OH **1993**, p. 218.
[20] L. J. Skipper, F. E. Sowrey, D. M. Pickup, K. O. Drake, M. E. Smith, P. Saravanapavan, L. L. Hench, R. J. Newport, *J. Mater. Chem.* **2005**, *15*, 2369.
[21] R. N. Mead, G. Mountjoy, *Chem. Mater.* **2006**, *18*, 3956.
[22] J. Du, A. N. Cormack, *J. Non-Cryst. Solids* **2004**, *349*, 66.
[23] M. Cerruti, V. Bolis, G. Magnacca, C. Morterra, *Phys. Chem. Chem. Phys.* **2004**, *6*, 2468.
[24] B. E. Warren, *X-Ray Diffraction*, Dover Publications, New York **1990**.
[25] J. M. Cole, E. R. H. van Eck, G. Mountjoy, R. Anderson, T. Brennan, G. Bushnell-Wye, R. J. Newport, G. A. Saunders, *J. Phys. Condens. Matter* **2001**, *13*, 4105.
[26] http://www.isis.rl.ac.uk/disordered/Manuals/gudrun/gudrun_-GEM.htm.
[27] R. L. McGreevy, L. Pusztai, *Mol. Simul.* **1988**, *1*, 359.